Low Temperature Physics/Fizyka Nyzkykh Temperatur, 2023, Vol. 49, No. 5, pp. 676–685

Ultra-low-noise transimpedance amplifier in cryogenic STM for studying novel quantum states by measuring shot noise

Ying-Xin Liang

Anyang Normal University, School of Physics and Electrical Engineering, Anyang 455000, Henan, China

E-mail: cryoliang@qq.com

Received September 8, 2022, published online March 22, 2023

An ultra-low-noise large-bandwidth transimpedance amplifier (TIA) for cryogenic scanning tunneling microscope (CryoSTM) is proposed. The TIA connected with the tip-sample component in CryoSTM is called as CryoSTM-TIA. Its transimpedance gain is as high as 1 GΩ, and its bandwidth is over 300 kHz, but its equivalent input noise current power spectral density is less than 4 $(\text{fA})^2/\text{Hz}$ at 100 kHz. The low inherent noise for the CryoSTM-TIA is due to its special design: (1) its pre-amplifier is made of a pair of low-noise cryogenic high electron mobility transistors (HEMTs); (2) the noise generated by one HEMT is eliminated by a large capacitor; (3) the capacitance of the cable connected the gate of the other HEMT to the tip is minimized; (4) thermal noise sources, such as the feedback resistor, are placed in the cryogenic zone. The dc output voltage drift of the CryoSTM-TIA is very low, as 5 μV/°C. The apparatus can be used for measuring the scanning tunneling differential conductance spectra, especially the scanning tunneling shot noise spectra (STSNS) of quantum systems, even if the shot noise is very low. It provides a universal tool to study various novel quantum states by measuring STSNS, such as detecting the Majorana bound states.

Keywords: cryogenic scanning tunneling microscope, transimpedance amplifier, high electron mobility transistor, equivalent input noise current power spectral density, scanning tunneling shot noise spectra, Majorana bound states.

1. Introduction

As the nonequilibrium transport statistics of the time-dependent fluctuations, shot noise yields information in mesoscopic systems that is not present in the time-averaged transport characteristics (differential conductance spectra) [1]. Therefore, shot noise has been a powerful tool to investigate novel quantum states in mesoscopic systems in experiments, such as verifying the statistical properties of anyons in fractional quantum Hall systems [2], studying the electron correlation mechanism of high-T_c superconductors [3–6], observing Andreev reflection [7, 8] and Kondo effect [9], etc.

Cryogenic scanning tunneling microscope (CryoSTM) has been used to measure shot noise in quantum systems at atomic scale [3, 4, 6, 8, 10, 11]. For measuring shot noise with CryoSTM, the amplifier as a key element must be able to work in high frequencies, since the pink noise component of the tunneling current noise is almost zero and the shot noise component becomes the dominant one in high frequencies. In addition, the amplifier inherent noise must be low enough to avoid disturbing the tunneling shot noise measurements. In Refs. 10, 11, it has been reported that the voltage amplifier containing an LC resonator in CryoSTM (denoted as CryoSTM-LC-Amp) is used to measure the tunneling shot noise. By CryoSTM-LC-Amp, only the signals at frequencies near the resonant one (1 MHz [10] or 3 MHz [11]) can be amplified with high gain. Some excellent works on high-T_c superconductors are performed with this apparatus [3, 4, 6]. However, the amplifier inherent noise, i.e., its equivalent input noise current power spectral density (PSD), is quite high, which is about 700 $(\text{fA})^2/\text{Hz}$, so it is difficult to obtain Fano factor accurately by measuring the very weak shot noise with this apparatus.

The theoretical works show that topological qubits can be constructed by Majorana bound states (MBSs), so the large-scale topological quantum computer will be realized by the arbitrary expansion for quantity of these qubits [12]. A lot of experimental works suggested the existence of MBSs based on the observed zero bias conductance peek (ZBCP) [13–16]. However, in spite of promising signatures, more mundane explanations still exist and the interpretation of the experiments continues to be debated [17]. For example,

Andreev bound states (ABSs) representing pairs of "fake" MBSs cannot be ruled out yet. Therefore, theorists have predicted the shot noise behaviors for some topological quantum systems in which MBSs may exist, to distinguish the MBSs from the "fake" ones [18–24]. However, the shot noise measurements for MBSs should be performed near the zero bias, which is about tens to hundreds μV, so the tunneling current I is quite small and the shot noise PSD $2Fe|I|$ is very weak. Up to now, no attempt is tried to measure the shot noise for MBSs, since no equipment meets their noise measurement accuracy.

Transimpedance amplifier (TIA) is the most commonly used amplifier in scanning tunneling microscopy/spectroscopy [25–27], amplifying the tunneling current signals to the output voltage signals. The TIA with the tip-sample component in CryoSTM is called as CryoSTM-TIA. In Ref. 28, a design of CryoSTM-TIA is proposed, whose transimpedance gain is 1 GΩ and bandwidth is more than 300 kHz, and its equivalent input noise current PSD is 21 $(\text{fA})^2/\text{Hz}$ at 100 kHz.

In this work, an improvement for the CryoSTM-TIA in Ref. 28 is proposed. The transimpedance gain of the proposed CryoSTM-TIA in this work is still as high as 1 GΩ and its bandwidth is still higher than 300 kHz, but its equivalent input noise current PSD is only 3 $(\text{fA})^2/\text{Hz}$ at 100 kHz, which is only 1/7 of the CryoSTM-TIA in Ref. 28. And the dc output voltage drift of the CryoSTM-TIA is very low, as 5 μV/°C. Therefore, in CryoSTM, the lower tunneling shot noise of quantum states can be measured at atomic scale with this apparatus.

2. Circuit of the proposed CryoSTM-TIA

Figure 1 shows the circuit of the proposed CryoSTM-TIA. It consists of four components: the pre-amplifier (Pre-Amp) shown in dashed box (a1) and dashed box (a2) in Fig. 1, the post-amplifier (Post-Amp) shown in dashed box (b), the compensated feedback network shown in dashed box (c), and the signal source circuit show in dashed box (d). The two-stage amplifier made of the Pre-Amp and Post-Amp is called as inverting-amplifier, denoted as Inv-Amp. The Inv-Amp is connected with the feedback network to form the TIA. The input N of the TIA is connected to the signal source circuit, to form the CryoSTM-TIA. The components placed in the cryogenic zone are shown in the dotted box. The parameters of all components of the CryoSTM-TIA circuit are listed in Table 1.

2.1. Design of Pre-Amp

The Pre-Amp is the same as that in Ref. 28. All parameters of the Pre-Amp are listed in Table 1. The differential amplifier part of the Pre-Amp is shown in dashed box (a1) in Fig. 1. H1 and H2 are cryogenic high electron mobility transistors (HEMTs), i.e., CNRS-HEMTs developed by CNRS/LPN in France [30, 31]. Its performance parameters are listed in Table 1, where $\overline{e_{\text{H}}^2}$ is the equivalent input noise voltage PSD of CNRS-HEMT, and $\overline{i_{\text{H}}^2}$ is its equivalent input noise current PSD [31]. In the circuit, $R_1 = R_2 = R_{\text{L}}$; R_{12} is a potentiometer, and $R_{12} \le 0.01R_{\text{L}}$; $R_{\text{L1}} = R_1 + \lambda R_{12}$ and $R_{\text{L2}} = R_2 + (1-\lambda)R_{12}$, and λ can vary from 0 to 1.

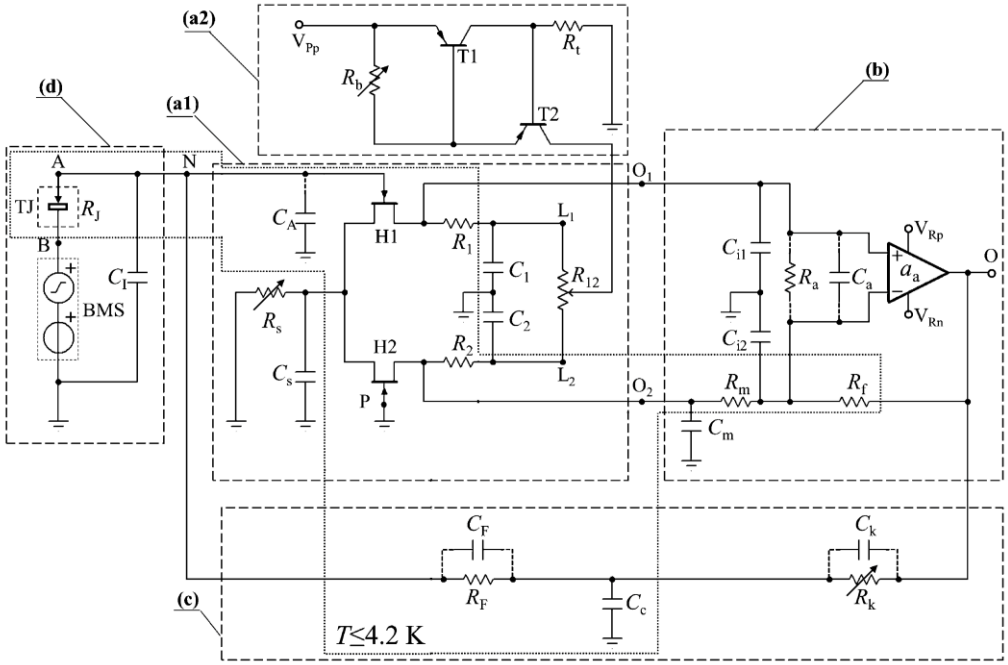

Fig. 1. Circuit of the proposed CryoSTM-TIA. Differential amplifier part of Pre-Amp is shown in dashed box (a1), constant-current source part of Pre-Amp in dashed box (a2), the Post-Amp in dashed box (b), the compensated feedback network in dashed box (c), and the signal source circuit in dashed box (d). The components placed in the cryogenic zone are shown in the dotted box. The parameters of all components of the CryoSTM-TIA circuit are listed in Table 1.

Table 1. Parameters of all components of CryoSTM-TIA circuit

CNRS-HEMTs H1 and H2			
Gate-source resistance R_A			> 10 TΩ
Transconductance g_m			40 mS
Channel conductance g_d			1 mS
Gate-source capacitance C_{gs}			5 pF
Gate-drain capacitance C_{gd}			1 pF
Drain-source voltage V_{ds}			100 mV
Drain-source current I_{ds}			1 mA
$\overline{e_H^2}$ [(nV)²/Hz]		10 kHz	0.25
		100 kHz	0.07
$\overline{i_H^2}$ [(fA)²/Hz]		10 kHz	0.1
		100 kHz	1
Pre-Amp			
R_s	(50 ± 1) Ω	C_s	0.1 mF
R_1 and R_2	1 kΩ	R_{12}	10 Ω
C_1 and C_2	10 μF		
T1 and T2	BJT BFT93 [29]	R_b	(347 ± 1) Ω
R_t	20 kΩ	V_{Pp}	+12 V
Post-Amp with THS4021 as Rear-OPA			
a_{a0}	97.5 dB	f_b	14.5 kHz
C_a	1.5 pF	R_a	1 MΩ
C_m	10 μF	R_m	500 Ω
R_f	1 MΩ	C_{i1} and C_{i2}	100 pF
Supply voltages V_{Rp}, V_{Rn}		+15, –15 V	
Feedback network			
R_F	1 GΩ	C_F	~ 0.3 pF
R_k	100 kΩ	C_k	~ 0.2 pF
C_c	3 nF		
Signal source circuit			
R_J	≥ 1 MΩ	C_I	~ 0.5 pF

Note: ± indicates the variable resistance range. For the simulations and calculations, without declaration, the default value after ± is 0.

Gate N of H1 as the Pre-Amp input is connected to the CryoSTM tip, and gate P of H2 is connected to ground permanently. R_A is the gate-source resistance of H1, and it is also the Pre-Amp input resistance. It is larger than 10 TΩ, so it can be considered as infinity. C_A is the Pre-Amp input capacitance. The capacitor C_s as the ac short-circuit capacitor is 0.1 mF, and the capacitors C_1 and C_2 as the ac short-circuit capacitors are 10 μF. H1, H2, R_1, and R_2 are placed in the cryogenic zone. H1 is placed as close as possible to the CryoSTM tip, to minimize the capacitance of the cable connected gate N of H1 to the tip. This capacitance is denoted as C_I, which is reduced to less than 0.5 pF. The voltage gain of the Pre-Amp A_{vP} in (0, 3 MHz] can be considered as a constant,

$$A_{vP} = -g_m R_d, \tag{1}$$

where $R_d = R_L / (1 + g_d R_L)$. The input capacitance of the Pre-Amp is

$$C_A = C_{gs} + (1 - A_{vP}) C_{gd}. \tag{2}$$

For the Pre-Amp, with the component parameters listed in Table 1, $R_d = 500$ Ω, $A_{vP} = -20$, and $C_A = 26$ pF.

In Fig. 1, the constant-current source part of the Pre-Amp is shown in the dashed box (a2). For a given resistance R_b, there is almost no fluctuation for the current I_{sour} generated by the constant-current source, even though the voltage V_{Pp} of the positive voltage source fluctuates greatly, which ensures the stability of the static operating point of H1 and H2.

2.2. Design of Post-Amp and composition of Inv-Amp

The Post-Amp circuit is shown in the dashed box (b) of Fig. 1. There is a commercial operational amplifier (OPA) in the circuit, called as Rear-OPA, which is THS4021 [32] in this work. R_a and C_a are the input resistance and capacitance of the Rear-OPA, respectively. The feedback resistor R_f is connected to the output of the Rear-OPA and its inverting input. R_f is 1 MΩ. There are two cables in the Post-Amp circuit. One cable connects output O_1 of the Pre-Amp and the noninverting input of the Rear-OPA, and the other one connects output O_2 of the Pre-Amp and the inverting input of the Rear-OPA through a resistor R_m of 500 Ω in the cryogenic zone. The capacitance of the two cables is C_{i1} and C_{i2}, respectively, and $C_{i1} = C_{i2} = C_i \approx 100$ pF. In this work, $C_i >> C_a$. O_2 is also connected with a ground short-circuit capacitor C_m of 10 μF, which is used to filter out the noises generated by H2 and R_2. R_m acts as the ac ground resistance at the inverting input of the Rear-OPA. Cascade the Pre-Amp and Post-Amp to form the Inv-Amp. The voltage gain of the Inv-Amp $a_A(f)$ is the ratio between the ac voltage at the output and the ac voltage at the input. Since the ac signals from one branch of the Pre-Amp are filtered out by C_m, the circuit topology of the Inv-Amp is totally different from that of the Macro-OPA in Ref. 28. In the Macro-OPA, the output impedance of the Pre-Amp acts as the ground impedance at the inverting input of the Rear-OPA. However, in the Inv-Amp in this work, as output O_2 of the Pre-Amp is shortened by C_m, R_m has to be added in the circuit as the ac ground resistance at the inverting input of the Rear-OPA. The voltage gain of the Inv-Amp $a_A(f)$ is expressed as

$$a_A = A_{vP} A_{vR}. \tag{3}$$

By the nodal analysis method, a_A can be obtained with the equations listed in Supplemental file 1 [33]. In [10 mHz, 3 MHz], $a_A(f)$ calculated by the nodal analysis method is almost identical with the results simulated by TINA-TI [34], which is shown in Supplemental file 1 [33]. And then, with A_{vP} expressed by Eq. (1), A_{vR} can be obtained by $A_{vR} = a_A / A_{vP}$.

The Post-Amp parameters are listed in Table 1. In $\max\left\{\frac{g_m}{2\pi C_s}, \frac{1}{2\pi R_s C_s}, \frac{1}{2\pi R_m C_m}, \frac{1}{2\pi R_m C_2}\right\} << f \le 3\,\text{MHz}$ (i.e., $64\,\text{Hz} << f \le 3\,\text{MHz}$),

$$A_{vR} \approx \frac{R_f}{R_m}\frac{Z_d}{R_d}\frac{1+j2\pi f R_m C_i}{1+\dfrac{R_f}{a_a R_m}+j2\pi f\dfrac{R_f C_i}{a_a}}, \tag{4}$$

where $Z_d = R_d/(1+j2\pi f R_d C_i)$ and a_a is the open-loop voltage gain of the Rear-OPA. For THS4021, a_a can be approximately expressed as $a_a = a_{a0}/(1+jf/f_b)$. In [1 kHz, 3 MHz], $a_A(f)$ calculated by Eqs. (2), (3), and (4) is almost identical with the simulation results with the parameters in Table 1 [33].

2.3. Frequency compensation of feedback loop

In order to increase the bandwidth of the CryoSTM-TIA, for the high feedback resistor R_F with parasitic capacitance C_F, frequency compensation must be used in feedback loop [28, 35]. In Ref. 35, it has been realized that the compensated feedback network is achieved to broaden the bandwidth to MHz in experiments. For the feedback network, with the component parameters listed in Table 1, $Z_F(f)$ can be considered as the impedance of the feedback network, which is

$$Z_F(f) \approx R_F/(1+j2\pi f R_k C_k),$$

where C_k is the parasitic capacitance of R_k [28, 35]. In (0, 1 MHz], $|Z_F(f)| \approx R_F/|1+j2\pi f R_k C_k| > R_F/1.008$ and $|Z_F(f)| \le R_F$, so it can be considered that $Z_F(f)$ is equal to R_F.

2.4. Circuit stability of the proposed CryoSTM-TIA

In Fig. 1, the signal source circuit is shown in the dashed box (d), and its parameters are shown in Table 1. The differential resistance of the tip-sample tunnel junction (TJ) in CryoSTM is R_J, which is limited to no less than $10^{-3}R_F$ in our design. The capacitance of TJ is C_J, which is in parallel with R_J. And C_J is estimated as several fF [28]. $C = C_A + C_I + C_J$ in this work. C_J is at least two orders of magnitude less than $C_A + C_I$, so it can be ignored in C and $C \approx C_A + C_I$. In Fig. 1, the source BMS provides the dc bias V_i and sinusoidal modulated signal voltage $\dot{V}_i$ for the CryoSTM-TIA. In the following simulation, C_I is always taken as 0.5 pF. The TIA connects the signal source circuit to form the CryoSTM-TIA. According to the circuit parameters in Table 1, the performances of the CryoSTM-TIA can be simulated by TINA-TI.

The loop gain T_L of the proposed CryoSTM-TIA [36] is

$$T_L(f) = -a_A(f)\beta(f) = -a_A(f)/[1/\beta(f)], \tag{5}$$

in which $\beta(f)$ is the feedback factor, and its reciprocal is

$$1/\beta(f) \approx 1 + Z_F[1/R_J + 1/R_A + j2\pi f(C_A + C_I)]. \tag{6}$$

For the Inv-Amp, Figs. 2(a) and 2(b) show the curves for $|a_A(f)|$ and $\angle(a_A(f))$ simulated by TINA-TI. By Eq. (6), $|1/\beta(f)|$ and $\angle(1/\beta(f))$ can be calculated. Fig. 2(a) shows the calculated results of $|1/\beta(f)|_{dB}$ and $\angle(1/\beta(f))$ with $R_J = +\infty$, and Fig. 2(b) shows those with

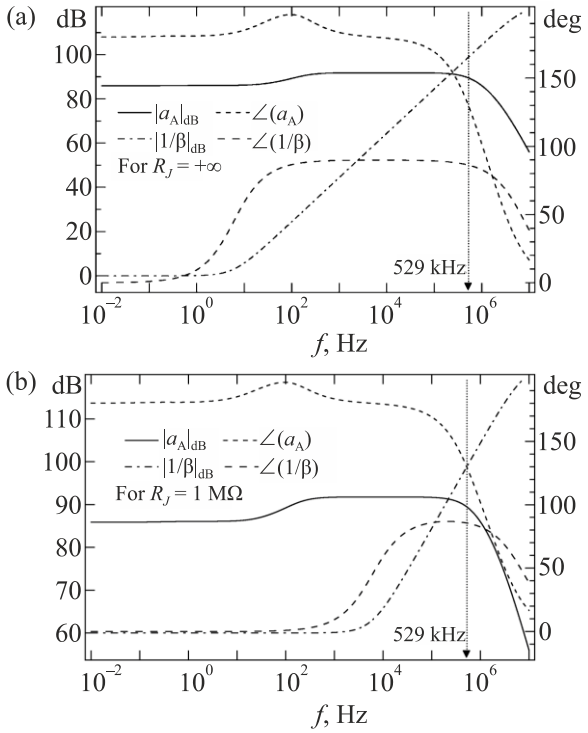

Fig. 2. TINA-TI simulation results for the voltage gain a_A of the Inv-Amp and $1/\beta(f)$ (a) with $R_J = +\infty$, (b) with $R_J = 1$ MΩ. Both figures show $|T_L|_{dB} = |a_A|_{dB} - |1/\beta(f)|_{dB} \le -10$ dB in $f \ge 529$ kHz and $\angle(T_L) = \angle(-a_A) - \angle(1/\beta) = \angle(a_A) - 180^\circ - -\angle(1/\beta) > -137^\circ$ in $f < 529$ kHz. Hence, the CryoSTM-TIA is stable enough.

$R_J = 1$ MΩ. Both figures show $|T_L|_{dB} = |a_A|_{dB} - -|1/\beta(f)|_{dB} \le -10$dB in $f \ge 529$kHz and $\angle(T_L) = \angle(-a_A) - -\angle(1/\beta) = \angle(a_A) - 180^\circ - \angle(1/\beta) > -137^\circ$ in $f < 529$kHz. Therefore, the CryoSTM-TIA is stable with gain margin more than 10 dB and phase margin more than 43° [37].

2.5. Voltage gain and transimpedance gain of the proposed CryoSTM-TIA

With the frequency compensation as mentioned in Sec. 2.3, it can be considered that Z_F is equal to R_F in (0, 1 MHz]. Considering the TJ capacitance C_J, the TJ impedance should be $Z_J = R_J/(1+j2\pi f R_J C_J)$. And $C \approx C_A + C_I$. As the ac input voltage $\dot{V}_i$ is applied by BMS, the output voltage of the CryoSTM-TIA is $\dot{V}_o$, and the voltage gain of the CryoSTM-TIA is $A_v = \dot{V}_o/\dot{V}_i$. By the nodal analysis method, in (0, 1 MHz],

$$A_v \approx -\frac{R_F}{Z_J}\frac{1}{1-\dfrac{1}{a_A}-\dfrac{R_F}{a_A R_J}-\dfrac{R_F}{a_A R_A}-j2\pi f\dfrac{R_F(C_A+C_I)}{a_A}}. \tag{7}$$

Setting $\dot{V}_i = 0$ and applying a sinusoidal current source $\dot{I}_i$ in parallel with TJ, the output voltage $\dot{V}_o$ is generated at the output of the CryoSTM-TIA. $A_i = \dot{V}_o/\dot{I}_i$ is called the transimpedance gain of the CryoSTM-TIA. In [0, 1 MHz],

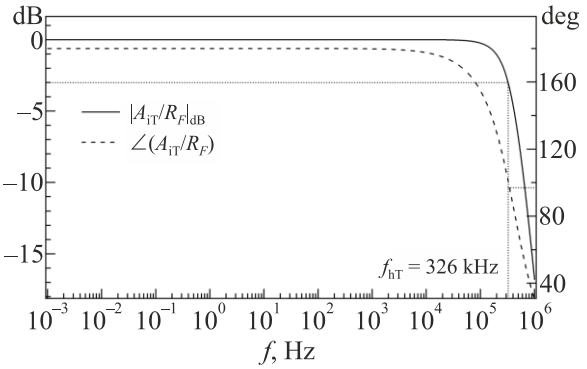

Fig. 3. TINA-TI simulation results for $A_{iT}(f)/R_F$, A_{iT} is the transimpedance gain of the TIA in the proposed CryoSTM-TIA. $|A_{iT}(f_{hT})/R_F|_{dB} = -3$ dB and $\angle(A_{iT}(f_{hT})/R_F) = 97^\circ$ at $f_{hT} = 326$ kHz.

$$A_i \approx -\frac{R_F}{1-\frac{1}{a_A}-\frac{R_F}{a_A R_J}-\frac{R_F}{a_A R_A}-j2\pi f\frac{R_F(C_A+C_I)}{a_A}}. \tag{8}$$

Disconnecting the TIA with the signal source circuit and applying a sinusoidal current source $\dot{I}_{iT}$ into the input of the TIA, the output voltage $\dot{V}_{oT}$ is generated at the output of the TIA. $A_{iT} = \dot{V}_{oT}/\dot{I}_{iT}$ is called the transimpedance gain of the TIA. In [0, 1 MHz],

$$A_{iT} = -\frac{R_F}{1-\frac{1}{a_A}-\frac{R_F}{a_A R_A}-j2\pi f\frac{R_F C_A}{a_A}}, \tag{9}$$

Figure 3 shows A_{iT}/R_F simulated by TINA-TI. The simulation results show that its –3 dB frequency is $f_{hT} = 326$ kHz. In addition, it is found that $|A_{iT}(f)/R_F|_{dB}$ decreases monotonically, and there is no "gain peaking" on the curve, which also indicates the circuit is quite stable [36]. In Supplemental file 3 [38], $|A_{iT}/R_F|_{dB}$ and $\angle(A_{iT}/R_F)$ calculated by Eq. (9) with the parameters in Table 1 are identical with the TINA-TI simulation results, which verifies the correctness of Eq. (9) for A_{iT}. Comparing Eqs. (8) and (9), as $C_A + C_I \approx C_A$ and $R_J \geq 10^{-3} R_F$, the upper cut-off frequency of the CryoSTM-TIA is approximately equal to f_{hT}, but a little bit smaller than f_{hT}.

2.6. Transient response of the proposed CryoSTM-TIA

The simulation results for the transient response of the proposed CryoSTM-TIA are shown in Supplemental file 4 [39]. For the CryoSTM-TIA, the time taken from adding the input step signal voltage to the output response stably within a certain error is called the transient response time t_r. For the simulations, a resistor with a constant resistance R_0 is instead of the tip-sample junction. When $R_0 \geq 30$ MΩ, for 0.1% error, $t_r < 3.5$ μs. When 3 MΩ $\leq R_0 <$ 30 MΩ, for 1% error, $t_r < 3.5$ μs. When 1 MΩ $\leq R_0 <$ 3 MΩ, for 3% error, $t_r < 3.5$ μs.

3. Inherent noise of the proposed CryoSTM-TIA

For the circuit of the proposed CryoSTM-TIA shown in Fig. 1, the differential equivalent circuit with all noise sources is used to calculate its equivalent input noise. The details for the noise calculations are shown in Supplemental file 5 [40].

3.1. Equivalent input voltage noise and equivalent input current noise of Inv-Amp

The equivalent input noise voltage and equivalent input noise current of H1 are denoted as e_H and i_H, respectively. The resistors R_1, R_2, and R_f are in the cryogenic zone of 4.2 K. The noises generated by R_1, R_2, and R_f in $f > 1$ kHz are thermal noise, and they can be neglected [28]. The noise voltage of the resistors R_m is denoted as e_m. The equivalent input noise voltage and equivalent input noise current of Rear-OPA are denoted as e_a and i_a, respectively. These noise sources are independent. The equivalent input noise voltage and equivalent input noise current of the Inv-Amp are denoted as e_A and i_A, respectively. By the nodal analysis method and Wiener–Sinchin theorem, ignoring the minor terms, it is obtained

$$\overline{e_A^2} = \overline{e_H^2} + \frac{\overline{e_m^2}+\overline{e_a^2}}{A_{vP}^2} + \left(1+\frac{R_m}{R_d}\right)^2 \frac{\overline{i_a^2}}{g_m^2}, \tag{10}$$

$$\begin{aligned}\overline{i_A^2} &= \overline{i_H^2} + (2\pi f)^2 C_A^2 \left(\overline{e_m^2}+\overline{e_a^2}\right)/A_{vP}^2 \\ &+ (2\pi f)^2 \left(C_{gs}+C_{gd}+C_A R_m/R_d\right)^2 \overline{i_a^2}/g_m^2,\end{aligned} \tag{11}$$

$$\begin{aligned}\overline{e_A i_A^*} &= (\overline{i_A e_A^*})^* = -j2\pi f C_A \left(\overline{e_m^2}+\overline{e_a^2}\right)/A_{vP}^2 \\ &- j2\pi f\left(C_{gs}+C_{gd}+\frac{R_m}{R_d}C_A\right)\left(1+\frac{R_m}{R_d}\right)\frac{\overline{i_a^2}}{g_m^2}.\end{aligned} \tag{12}$$

According to the parameters of the Inv-Amp listed in Table 1, $\overline{e_A^2} = 0.27$ (nV)²/Hz and $\overline{i_A^2} = 0.13$ (fA)²/Hz at $f = 10$ kHz, and $\overline{e_A^2} = 0.08$ (nV)²/Hz and $\overline{i_A^2} = 2.7$ (fA)²/Hz at $f = 100$ kHz. For the Macro-OPA in Ref. 28, $\overline{e_A^2}$ = = 0.5 (nV)²/Hz and $\overline{i_A^2} = 0.8$ (fA)²/Hz at $f = 10$ kHz, and $\overline{e_A^2} = 0.14$ (nV)²/Hz and $\overline{i_A^2} = 20$ (fA)²/Hz at $f = 100$ kHz. Comparing the Macro-OPA in Ref. 28, the output of H2 in the Inv-Amp is grounded through the large capacitor C_m, so the high-frequency noises generated by H2 and R_2 are filtered out. In this work, R_m is added, but its resistance is only 500 Ω and it is placed in the cryogenic zone. The noise generated by R_m is three orders of magnitude smaller than that generated by H2 in Ref. 28, i.e., $\overline{e_m^2} << A_{vP}^2 \overline{e_H^2}$. Therefore, the equivalent input noises of the Inv-Amp are much lower than those of the Macro-OPA in Ref. 28.

$\overline{e_a^2} = 2.25$ (nV)^2/Hz and $\overline{i_a^2} = 4$ (pA)^2/Hz in $f \geq 10$ kHz [32]. In Eqs. (10), (11), and (12), $\overline{e_m^2}$ is one order of magnitude smaller than $\overline{e_a^2}$. In Eq. (10), $\left(1+\frac{R_m}{R_d}\right)^2 \frac{\overline{i_a^2}}{g_m^2}$ is one order of magnitude smaller than $\overline{e_H^2}$. In Eq. (11), $\left(C_{gs}+C_{gd}+C_A R_m / R_d\right)^2 \overline{i_a^2} / g_m^2$ is one order of magnitude smaller than $C_A^2 \overline{e_a^2} / A_{vP}^2$. In Eq. (12), $\left(C_{gs}+C_{gd}+\frac{R_m}{R_d} C_A\right) \times \left(1+\frac{R_m}{R_d}\right) \frac{\overline{i_a^2}}{g_m^2}$ is one order of magnitude smaller than $C_A \overline{e_a^2} / A_{vP}^2$. Further ignoring the minor terms in Eqs. (10), (11), and (12),

$$\overline{e_A^2} = \overline{e_H^2} + \overline{e_a^2} / A_{vP}^2, \tag{13}$$

$$\overline{i_A^2} = \overline{i_H^2} + (2\pi f)^2 C_A^2 \overline{e_a^2} / A_{vP}^2, \tag{14}$$

$$\overline{e_A i_A^*} = (\overline{i_A e_A^*})^* = -j2\pi f C_A \overline{e_a^2} / A_{vP}^2. \tag{15}$$

3.2. Equivalent input current noise of the proposed CryoSTM-TIA

The equivalent input noise current PSD of the proposed CryoSTM-TIA is obtained as

$$\begin{aligned}\overline{i_{in}^2} = \overline{i_A^2} + 4k_B T / R_F + \left[1/R_J^2 + 1/R_F^2 + (2\pi f)^2 C_{IJ}^2\right] \overline{e_A^2} \\ + \left(1/R_J + j2\pi f C_{IJ}\right)\left(\overline{e_A i_A^*} + \overline{e_A^2} / R_F\right) \\ + \left(1/R_J - j2\pi f C_{IJ}\right)\left(\overline{i_A e_A^*} + \overline{e_A^2} / R_F\right),\end{aligned} \tag{16}$$

where $C_{IJ} = C_I + C_J$ [28, 40]. Putting Eqs. (13), (14), and (15) into Eq. (16), so

$$\begin{aligned}\overline{i_{in}^2} = \overline{i_H^2} + 4k_B T / R_F + \left(1/R_J + 1/R_F\right)^2 \left(\overline{e_H^2} + \overline{e_a^2} / A_{vP}^2\right) \\ + (2\pi f)^2 \left(C_{IJ}^2 \overline{e_H^2} + C^2 \overline{e_a^2} / A_{vP}^2\right),\end{aligned} \tag{17}$$

i.e.,

$$\overline{i_{in}^2} = \overline{i_A^2} + 4k_B T / R_F + \left(1/R_J + 1/R_F\right)^2 \overline{e_A^2} + \overline{i_{CIJ}^2}, \tag{18}$$

where $\overline{i_{CIJ}^2} = (2\pi f)^2 (C_{IJ}^2 \overline{e_A^2} + 2C_A C_{IJ} \overline{e_a^2} / A_{vP}^2)$.

For the proposed CryoSTM-TIA, $R_F = 1$ GΩ, $C_A = 26$ pF, $C_I = 0.5$ pF, and $C_J = 10$ fF. R_F and TJ are in the cryogenic zone at 4.2 K. As $R_J = 1$ MΩ, $\overline{i_{in}^2}$ and its four components are listed in Table 2. The noise components of the CryoSTM-TIA in Ref. 28 are also shown in Table 2. The CryoSTM-TIA proposed in this work has an equivalent input noise current PSD of 0.6 (fA)^2/Hz at 10 kHz and 3 (fA)^2/Hz at 100 kHz, which is much lower than that in Ref. 28.

Table 2. Noise components of CryoSTM-TIAs

TIA type	in this work		in Ref. 28	
f, kHz	10	100	10	100
$\overline{e_A^2}$, (nV)^2/Hz	0.27	0.08	0.5	0.14
Unit for the following terms is (fA)^2/Hz				
$\overline{i_A^2}$	0.13	2.7	0.8	20
$4k_B T / R_F$	0.2	0.2	0.2	0.2
$\overline{i_{CIJ}^2}$	0.0013	0.06	0.03	0.7
$\left(\frac{1}{R_J}+\frac{1}{R_F}\right)^2 \overline{e_A^2}$	0.26	0.08	0.5	0.14
$\overline{i_{in}^2}$ as total	0.6	3	1.5	21

4. CryoSTM-TIA operating state adjustment and dc tunneling current measurement

For the proposed CryoSTM-TIA, CNRS-HEMTs H1 and H2 should be selected with the same performances, as far as possible.

Disconnect the Pre-Amp from the Post-Amp, and ground the Pre-Amp input N. Adjust potentiometer R_{12} to $R_{L1} = R_{L2}$. Adjust the current generated by the constant-current source in dashed box (a2) in Fig. 1 to $I_{sour} = 2$ mA. Adjust the resistance R_s to achieve the gate-source voltage V_{gs} of H1 and H2 for their operating points near the ideal one ($V_{ds} = 100$ mV and $I_{ds} = 2$ mA), as far as possible.

Cascade the Pre-Amp and Post-Amp to form the Inv-Amp. Then, the dc voltage V_{om} at the output of the Inv-Amp is called as the output offset voltage of the Inv-Amp. As H1 and H2 are identical, V_{om} is caused by the following factors: the common-mode dc voltages on the inputs of the Rear-OPA [32, 41] in the Post-Amp, its input offset voltage, its input bias currents, and its input offset current. Usually, V_{om} is not 0. For the voltage gain of the Inv-Amp $a_A(f)$, when $f \to 0$, $a_A \to a_{A0}$. a_{A0} is the dc voltage gain of the Inv-Amp. And $|a_{A0}|_{dB} \approx |A_{vP} R_f / (R_m + R_d)|_{dB} = 86$ dB, which is consistent with the simulation result of $|a_{A0}|_{dB} = 85$ dB [33]. V_{om} can be considered as $V_{om} = a_{A0} V_{OS}$, where V_{OS} is the input offset voltage of the Inv-Amp, as shown in Fig. 4. Since the input resistances of H1 and H2 can be considered as infinity, the input bias currents and input offset current of the Inv-Amp can be considered as 0. $|V_{OS}|$ is estimated to be 60 μV, and the drift of V_{OS} is only 5 μV/°C. How to estimate V_{OS} and its drift are presented in Supplemental file 6 [41]. The power of the constant-current source is about 24 mW. As a common means in industry, a simple temperature control system based on the TEC devices [42] can be used to control the temperature fluctuations of the constant-current source within 0.1 °C [43] and those of Rear-OPA within 1 °C, so the fluctuations of V_{OS} within 1 μV are guaranteed.

The dissimilarities of H1 and H2 cannot affect the TIA ac performances, since the ac signals from one branch of

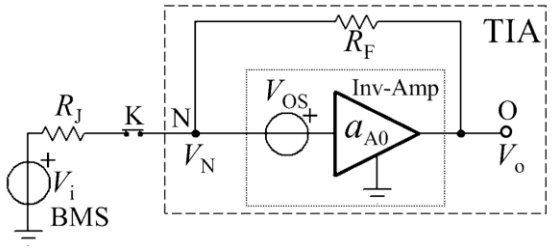

Fig. 4. Scheme of dc circuit of the proposed CryoSTM-TIA. V_{OS} is the input offset voltage of the Inv-Amp.

the Pre-Amp is filtered out by C_m. And, as the differences in the performances of H1 and H2 are small enough, $|V_{OS}|$ induced by the dissimilarities of H1 and H2 can be adjusted to 0 by adjusting R_{12}, and the drift of V_{OS} can be controlled with the better temperature control system [44].

Connect input N to the output of the Inv-Amp with the feedback resistor $R_F + R_k \approx R_F$, and then disconnect it from ground, to form the TIA, as shown in Fig. 4. Here, switch K is off, i.e., the signal source circuit is disconnected. The output voltage of the TIA is V_{tia}, which is equal to the voltage at the TIA input N. For V_{tia},

$$a_{A0}(V_{tia} + V_{OS}) = V_{tia}. \tag{19}$$

Therefore, $V_{OS} = V_{tia}(1 - a_{A0})/a_{A0}$ is almost equal to $-V_{tia}$. V_{tia} can be measured. And $|V_{tia}|$ can be lowered by adjusting R_{12}, even to 0.

Switch on switch K, i.e., the signal source circuit is connected to the TIA, to form the CryoSTM-TIA, as shown in Fig. 4. As the dc bias V_i is applied by BMS, the dc resistance of TJ is R, and the potential at input N is V_N, and the output voltage of the CryoSTM-TIA is V_o. Obviously, $a_{A0}(V_N + V_{OS}) = V_o$, and $(V_i - V_N)/R = (V_N - V_o)/R_F$. The dc bias on TJ is $V = V_i - V_N$, and dc tunneling current $I = (V_i - V_N)/R$. I_s as an approximate value of the dc tunneling current I is

$$I_s = -(V_o - V_{tia})/R_F. \tag{20}$$

The relative error is obtained as

$$\mathrm{Er} = |I_s - I|/|I| = 1/(1 - a_{A0}),$$

and the dc bias on TJ is obtained as

$$V = V_i - V_{tia} + (V_{tia} - V_o)/a_{A0}. \tag{21}$$

As $|a_{A0}|_{dB} \approx 85$ dB, $\mathrm{Er} < 57$ ppm, consistent with the simulation results [45]. By Eq. (20), $V_{tia} - V_o = R_F I_s \approx \approx R_F I = R_F V/R$. By Eq. (21), $V \approx V_i - V_{tia} + R_F V/(Ra_{A0})$, so $[1 - R_F/(Ra_{A0})]V \approx V_i - V_{tia}$. As the minimum of R_J is not less than 1 MΩ, $R \geq 1$ MΩ, so $|R_F/(Ra_{A0}| \leq 1/17$. Therefore, $V \approx V_i - V_{tia}$. Thus, with the measured V_{tia} and V_o, I_s and V can be obtained. By this means, the scanning tunneling current spectra $I = I(V)$ $(V \in [V_L, V_H])$ can be accurately obtained, where V_L and V_H are the lower limit and upper limit voltages for the measurements, respectively. As mentioned above, $V_{tia} \approx -V_{OS}$, so the fluctuations of V_{tia} can be controlled within 1 μV with the temperature control system. Therefore, excluding the fluctuations of V_i provided by BMS, the fluctuations of V are within 1 μV.

5. Applications in spectra measurements

For most applications, the modulus of the transimpedance gain of the CryoSTM-TIA $|A_i(f)|$ should be measured firstly. $A_i(f)$ is expressed as Eq. (8). Since $|a_A(f)|_{dB} > 90$ dB in [1 kHz, 300 kHz] as shown in Fig. 2, when $R_J \geq 10^{-3} R_F$, $|A_i(f)|$ in [1 kHz, 300 kHz] can be approximately expressed as

$$|A_i(f)| = R_F/|1 - j2\pi f R_F(C_A + C_I)/a_A(f)|. \tag{22}$$

How to measure it has been described in Ref. 28.

5.1. Measuring scanning tunneling differential conductance spectra

The differential conductance of TJ $G_J = 1/R_J$ is the function of the voltage V applied to TJ. As the frequency f of the modulated signal voltage $\dot{V}_i$ is low enough, such as $f < 1$ kHz, by Eq. (7),

$$A_v \approx -\frac{R_F}{R_J(V)} \cdot \frac{1}{1 - \dfrac{R_F}{a_A(f) R_J(V)}}.$$

Therefore, $R_J(V) \approx [1/a_A(f) - 1/A_v]R_F$. As $|a_A(f)|_{dB} > 85$ dB in $f \leq 300$ kHz as shown in Fig. 2, when the measured $|A_v| \leq 1000$, $R_J(V) \approx R_F/|A_v|$. $|A_v| = |\dot{V}_o|/|\dot{V}_i|$ can be measured, so the differential conductance spectra $G_J(V) = 1/R_J(V)$ $(V \in [V_L, V_H])$ can be obtained with the measured $|A_v|$.

Increasing the frequency of the modulated signal can speed up the differential conductance spectra measurements. In [1 kHz, 300 kHz], as $R_J \geq 1$ MΩ, by Eq. (7),

$$|A_v(f)| \approx \frac{1}{|Z_J(f)|} \cdot \frac{R_F}{|1 - j2\pi f R_F(C_A + C_I)/a_A(f)|}.$$

Therefore, $1/|Z_J(f)| \approx |A_v(f)|/|A_i(f)|$, where $|A_i(f)|$ is shown by Eq. (22). And, $|A_v(f)|$ and $|A_i(f)|$ can be measured. $1/|Z_J(f)| = \sqrt{1/R_J^2 + (2\pi f C_J)^2}$ can be obtained. Selecting two different frequencies f_1 and f_2 in [1 kHz, 300 kHz], $|Z_J(f_1)|$ and $|Z_J(f_2)|$ are obtained. R_J and C_J can be solved out from the measured $|Z_J(f_1)|$ and $|Z_J(f_2)|$.

Since the inherent noise of the CryoSTM-TIA is very small, the amplitude of the modulated signal voltage $\dot{V}_i$ can be very small (≤ 10 μV), so that the energy resolution for the STS measurements is much improved.

5.2. Measuring scanning tunneling shot noise spectra

The measurement method for the tunneling shot noise spectra is basically the same as that introduced by Ref. 28, and it is only briefly described as below.

Before approaching the tip to sample in the CryoSTM, R_J can be considered as infinity and C_J as 0. In this case,

the output noise voltage PSD of the CryoSTM-TIA $S_{su}(f)$ can be measured, and the equivalent input noise current PSD $\overline{i_i^2}(f)$ is

$$\overline{i_i^2}(f) = S_{su}(f)/|A_i(f)|^2, \quad (23)$$

where $|A_i(f)|$ is obtained by Eq. (22).

To measure the scanning tunneling shot noise spectra (STSNS) of a quantum system with the CryoSTM-TIA, the distance between the tip and sample is adjusted, so that the shot noise measurements in the selected domain $D_V = = \{V \mid V_L \le V \le V_H, G_J(V) < 1\mu S\}$ are performed [28]. In D_V, the output noise voltage PSD $S_{sum}(f,V)$ can be measured. The tunneling noise current PSD is denoted as $S_I(f,V)$. The equivalent input noise current PSD of the CryoSTM-TIA is the function of R_J, so it is the function of V and denoted as $\overline{i_{in}^2}(f,V)$. For $S_{sum}(f,V)$,

$$S_{sum}(f,V) = \left[S_I(f,V) + \overline{i_{in}^2}(f,V)\right]|A_i(f)|^2. \quad (24)$$

With Eqs. (23) and (24), it is obtained that

$$S_I(f,V) = \frac{S_{sum}(f,V) - S_{su}(f)}{|A_i(f)|^2} - [\overline{i_{in}^2}(f,V) - \overline{i_i^2}(f)].$$

From Eq. (18),

$$\overline{i_i^2}(f) = \overline{i_A^2} + \frac{4k_BT}{R_F} + \frac{\overline{e_A^2}}{R_F^2} + (2\pi f)^2\left(C_I^2\overline{e_A^2} + 2C_AC_I\frac{\overline{e_a^2}}{A_{vP}^2}\right).$$

$\overline{i_{in}^2}(f,V)$ is shown in Eq. (18). According to Table 1, $\delta(f,V)$ as the difference between $\overline{i_{in}^2}(f,V)$ and $\overline{i_i^2}(f)$ is smaller than 0.3 (fA)^2/Hz in [10 kHz, 100 kHz) and 0.1 (fA)^2/Hz in [100 kHz, 300 kHz]. $\delta(f,V)$ can be neglected compared with $S_I(f,V)$, so long as the minimum of $G_J(V)$ ($V \in D_V$) is not too small. Therefore, $S_I(f,V)$ can be obtained as

$$S_I(f,V) \approx \frac{S_{sum}(f,V) - S_{su}(f)}{|A_i(f)|^2},$$

with the measured $S_{sum}(f,V)$, $S_{su}(f)$, and $|A_i(f)|$. And then, the SNTNS $S_{Is}(I) = 2Fe|I|$ can be extracted from $S_I(f,V)$. Here, $I = I(V)$ ($V \in D_V$), and I is the dc tunneling current as the bias V is applied.

5.3. Detecting Majorana bound states by measuring shot noise

In Ref. 15, several evidences with ZBCP were provided for the existence of the vortex MBSs in iron-based superconductors, and they ruled out other nine possible mechanisms for ZBCP. For example, the occurrence of incoherent multiple Andreev reflection is ruled out by weak tunnel coupling conditions in CryoSTM (i.e., the tunnel junction resistance is large enough) [46]. The existence of the MBSs can be further verified by measuring the shot noise. The shot noise measurements by using the proposed CryoSTM-TIA can be performed as follows. As the iron-based superconductor sample is placed in the cryogenic zone of 0.55 K with a magnetic field of 2.5 T, the superconducting gap Δ is about 1.8 meV, and $4k_BT/e = 0.2$ mV. Under the different tunnel junction conductance (denoted as G_N in Ref. 15) conditions, the tunneling current spectra and tunneling differential conductance spectra are measured, and the results are shown as Fig. 3(A) in Ref. 15 and Figs. S1(A) and (B) in the supplemental file of Ref. 15. Taking the bias interval $[V_L, V_H]$ as $[4k_BT/e, \Delta/e] = [0.2\text{ mV}, 1.8\text{ mV}]$, we can select a condition that G_N is sufficiently low, such as $G_N = = 10\times10^{-3}G_0 \approx 0.77$ μS ($G_0 = 2e^2/h$), so that the minimum value of the corresponding tunneling differential conductance spectra is not more than $G_H = 1$ μS and not less than $G_L = 0.2$ μS. (For simplicity, the case of $[V_L, V_H]$ as $[-\Delta/e, -4k_BT/e]$ is not discussed in this work.) A domain $D_V = \{V \mid V_L \le V \le V_H, G_L \le G_J(V) \le G_H\}$ can be found under this measurement condition. Selecting a bias interval $[V_1,V_2] \subset D_V$ as long as possible, measure $S_I(f,V_1)$ and $S_I(f,V_2)$ ($f \in [10\text{ kHz}, 300\text{ kHz}]$) with the procedures mentioned in Sec. 5.2, and find their corner frequencies f_{1c} and f_{2c}, respectively. At the frequency $f_m = 10\max\{f_{1c}, f_{2c}\}$, $S_I(f_m,V)$ ($V \in [V_1,V_2]$) can be considered as white noise $S_{Iw}(V)$. And, in $[V_1,V_2]$, the shot noise $S_{Is}(V) = = S_{Iw}(V) \approx S_I(f_m,V)$. With the tunneling current spectra $I = I(V)$ ($V \in [V_1,V_2]$), the STSNS $S_{Is}(I) = 2FeI$ ($I = I(V)$, $V \in [V_1,V_2]$) are obtained, and then Fano factor can be extracted from the STSNS.

For measuring the STSNS for the vortex MBSs described in Ref. 15, as the tunneling bias V is in $[V_L, V_H] = [0.2\text{ mV}, 1.8\text{ mV}]$, the tunneling current $I = \int_0^V G_J(V)dV$. Because the minimum value of $G_J(V)$ is not less than $G_L = 0.2$ μS, $I \ge G_LV_L = 40$ pA in $[V_L, V_H]$. The Fano factor F is not necessarily a constant, so enough points should be measured for STSNS. If 100 points are selected in $[V_L, V_H]$, the step interval ΔV is 16 μV, and the corresponding ΔI may be only 3.2 pA. As mentioned in Sec. 4, the fluctuations of V can be controlled within 1 μV with the temperature control system, much less than ΔV, so the accuracy for V is guaranteed. For ΔI, the corresponding increment of the Poisson noise $2e(\Delta I)$ may be smaller than 1 (fA)^2/Hz, and the shot noise for the vortex MBSs are usually sub-Poisson noise. As the inherent noise of the CryoSTM-LC-Amp mentioned in Ref. 10 is about 700 (fA)^2/Hz, the measurement accuracy with the CryoSTM-LC-Amp is obviously far from meeting the accuracy requirements for measuring the STSNS for vortex MBSs. For the CryoSTM-TIA proposed in Ref. 28, whose inherent noise is 21 (fA)^2/Hz at 100 kHz and $\delta(f,V) << 0.28$ (fA)^2/Hz at 100 kHz, its measurement accuracy is barely acceptable. The CryoSTM-TIA proposed in this work, whose inherent noise is only 3 (fA)^2/Hz at 100 kHz and $\delta(f,V) < 0.1$ (fA)^2/Hz at 100 kHz,

its measurement accuracy can meet the accuracy requirements for measuring the STSNS for vortex MBSs with high precision.

For the above 2-terminal systems (the STM tip as one terminal and sample as the other one), the tunneling noise corner frequency is usually small, so the shot noise measurements are easily performed. By the same means, the STSNS for MBSs in 2D topological insulator/superconductor heterojunction systems [14] and in ferromagnetic chain/superconductor systems [13, 20] can also be investigated. In these systems, the evidences with ZBCP have been provided for the existence of MBSs. Ref. 20 also predicted in theory that Fano factor is a constant of 0.5 for MBS with the STSNS in $V > 4k_{\mathrm{B}}T/e$.

6. Conclusions

In this work, a design of transimpedance amplifier (TIA) for cryogenic STM (CryoSTM) is presented. The TIA connected with the tip-sample component in CryoSTM is called as CryoSTM-TIA. The Macro-OPA of the TIA in Ref. 28 is replaced with the Inv-Amp in this work. The Pre-Amp in the Inv-Amp is the same as that of the Macro-OPA in Ref. 28. But, the noninverting output of the Pre-Amp in the Inv-Amp is ac grounded through a large capacitor C_{m}, and it is connected with the inverting input of the Rear-OPA in the Post-Amp through a small resistor R_{m} as the ac ground resistance at the inverting input of the Rear-OPA. The ac signals from one branch of the Pre-Amp are filtered out by C_{m}, so the circuit topology of the Inv-Amp is totally different from that of the Macro-OPA in Ref. 28. And the noises generated from this branch of the Pre-Amp as ac signals are filtered out by C_{m}. Therefore, the CryoSTM-TIA still has transimpedance gain of 1 GΩ and bandwidth more than 300 kHz, but its inherent noise is reduced to 3 $(\mathrm{fA})^2/\mathrm{Hz}$ at 100 kHz (only 1/7 of that in Ref. 28). With this apparatus, the fast high-energy-resolution scanning tunneling spectra measurements can be performed and the very low tunneling shot noise of quantum systems can be measured with higher precision, so it is more universal in applications, compared with the apparatus mentioned in Ref. 28. This apparatus can be applied to study the novel physical properties of various quantum systems, such as detecting the existence of Majorana bound states in the topological quantum systems.

Acknowledgment

This work is supported by Open Research Fund Program of the State Key Laboratory of Low-Dimensional Quantum Physics (Grant No. KF202212). I acknowledge stimulating discussions with Prof. Fang-Hao Liang of Math. School in Shandong University and Prof. Xing Liang of Math. School in USTC.

Declaration of competing interest

The author declares that they have no known competing financial interests or personal relationships that could have appeared to influence the work reported in this paper.

1. Y. M. Blanter and M. Büttiker, *Phys. Rep.* **336**, 1 (2000).
2. H. Bartolomei, M. Kumar, R. Bisognin, A. Marguerite, J. M. Berroir, E. Bocquillon, B. Placais, A. Cavanna, Q. Dong, U. Gennser, Y. Jin, and G. Fève, *Science* **368**, 173 (2020).
3. K. M. Bastiaans, D. Cho, T. Benschop, I. Battisti, Y. Huang, M. S. Golden, Q. Dong, Y. Jin, J. Zaanen, and M. P. Allan, *Nat. Phys.* **14**, 1183 (2018).
4. F. Massee, Y. K. Huang, M. S. Golden, and M. Aprili, *Nat. Commun.* **10**, 544 (2019).
5. P. P. Zhou, L. Y. Chen, Y. Liu, I. Sochnikov, A. T. Bollinger, M. G. Han, Y. M. Zhu, X. He, I. Božović, and D. Natelson, *Nature* **572**, 493 (2019).
6. K. M. Bastiaans, D. Chatzopoulos, J. F. Ge, D. Cho, W. O. Tromp, J. M. van Ruitenbeek, M. H. Fischer, P. J. De Visser, D. J. Thoen, E. F. C. Driessen, T. M. Klapwijk, and M. P. Allan, *Science* **374**, 608 (2021).
7. F. Lefloch, C. Hoffmann, M. Sanquer, and D. Quirion, *Phys. Rev. Lett.* **90**, 067002 (2003).
8. K. M. Bastiaansa, D. Cho, D. Chatzopoulos, M. Leeuwenhoek, C. Koks, and M. P. Allan, *Phys. Rev. B* **100**, 104506 (2019).
9. T. Delattre, C. Feuillet-Palma, L. G. Herrmann, P. Morfin, J. M. Berroir, G. Fève, B. Placais, D. C. Glattli, M. S. Choi, C. Mora, and T. Kontos, *Nat. Phys.* **5**, 208 (2009).
10. F. Massee, Q. Dong, A. Cavanna, Y. Jin, and M. Aprili, *Rev. Sci. Instrum.* **89**, 093708 (2018).
11. K. M. Bastiaans, T. Benschop, D. Chatzopoulos, D. Cho, Q. Dong, Y. Jin, and M. P. Allan, *Rev. Sci. Instrum.* **89**, 093709 (2018).
12. S. Das Sarma, M. Freedman, and C. Nayak, *npj Quantum Inf.* **1**, 15001 (2015).
13. S. Nadj-Perge, I. K. Drozdov, J. Li, H. Chen, S. J. Jeon, J. P. Seo, A. H. MacDonald, B. A. Bernevig, and A. Yazdani, *Science* **346**, 602 (2014).
14. H. H. Sun, K. W. Zhang, L. H. Hu, C. Li, G. Y. Wang, H. Y. Ma, Z. A. Xu, C. L. Gao, D. D. Guan, Y. Y. Li, C. H. Liu, D. Qian, Y. Zhou, L. Fu, S. C. Li, F. C. Zhang, and J. F. Jia, *Phys. Rev. Lett.* **116**, 257003 (2016).
15. D. F. Wang, L. Y. Kong, P. Fan, H. Chen, S. Y. Zhu, W. Y. Liu, L. Cao, Y. J. Sun, S. X. Du, J. Schneeloch, R. D. Zhong, G. D. Gu, L. Fu, H. Ding, and H. J. Gao, *Science* **362**, 333 (2018).
16. B. Jäck, Y. L. Xie, and A. Yazdani, *Nat. Rev. Phys.* **3**, 541 (2021).
17. S. Frolov, *Nature* **592**, 351 (2021).
18. C. J. Bolech and E. Demler, *Phys. Rev. Lett.* **98**, 237002 (2007).
19. A. Golub and B. Horovitz, *Phys. Rev. Lett.* **83**, 153415 (2011).
20. H. Soller and A. Komnik, *Physica E* **63**, 99 (2014).
21. D. E. Liu, M. Cheng, and R. M. Lutchyn, *Phys. Rev. B* **91**, 081405 (2015).

22. C. W. J. Beenakker and D. O. Oriekhov, *SciPost Phys.* **9**, 080 (2020).
23. J. Manousakis, C. Wille, A. Altland, R. Egger, K. Flensberg, and F. Hassler, *Phys. Rev. Lett.* **124**, 096801 (2020).
24. A. M. Calle, P. A. Orellana, and J. A. Otalora, *Annalen der Physik* **533**, 2100040 (2021).
25. C. J. Chen, *Introduction to Scanning Tunneling Microscopy*, Oxford Univ. Press (1993), Chapt. 11.
26. Q. F. Li, Q. Wang, Y. B. Hou, and Q. Y. Lu, *Rev. Sci. Instrum.* **83**, 043706 (2012).
27. J. F. Ge, M. Ovadia, and J. E. Hoffman, *Rev. Sci. Instrum.* **90**, 101401 (2019).
28. Y. X. Liang, *Ultramicroscopy* **234**, 13466 (2022).
29. Data sheet of BFT93 BJT [Online], https://www.nxp.com.cn/docs/en/data-sheet/BFT93_CNV.pdf.
30. Y. X. Liang, Q. Dong, M. C. Cheng, U. Gennser, A. Cavanna, and Y. Jin, *Appl. Phys. Lett.* **99**, 113505 (2011).
31. Y. Jin, Q. Dong, A. Cavanna, U. Gennser, L. Couraud, and C. Ulysse, *Specific HEMTs for deep cryogenic high-impedance ultra low low-frequency noise read-out electronics*, in *12th IEEE International Conference on Solid-State and Integrated Circuit Technology (ICSICT)*, Grenoble, France, 7–9 July 2014.
32. Data sheet of THS4021 OPA [Online], https://www.ti.com/lit/ds/symlink/ths5021.pdf.
33. Supplimental file 1.
34. TINA-TI is SPICE-based analog simulation program produced by Texas Instruments Inc. [Online], https://www.ti.com/tool/TINA-TI.
35. B. Michel, L. Novotny, and U. Dürig, *Ultramicroscopy* **42-44**, 1647 (1992).
36. S. Franco, *Design with Operational Amplifiers and Analog Integrated Circuit*, McGraw-Hill Companies Inc. (2002).
37. Supplimental file 2.
38. Supplimental file 3.
39. Supplimental file 4.
40. Supplimental file 5.
41. Supplimental file 6.
42. A suitable TEC device [Online], https://datasheets.maximintegrated.com/en/ds/MAX1978-MAX1979.pdf.
43. Y. Mu, T. L. Hu, C. Chen, H. Gong, S. J. Li, *Infrared and Laser Engineering* **48**, 0405001 (2019).
44. W. Zhang, Z. L. Li, P. Guo, and J. Y. Zhao, *Semicond. Optoelectron.* **41**, 560 (2020).
45. Supplimental file 7.
46. L. Y. Kong and H. Ding, *Acta. Phys. Sin.* **69**, 110301 (2020).

Наднизькошумовий підсилювач трансімпедансу в кріогенному СТМ для вивчення нових квантових станів шляхом вимірювання дробового шуму

Ying-Xin Liang

Запропоновано наднизькошумовий з великою шириною полоси частот підсилювач трансімпедансу (TIA) для кріогенного скануючого тунельного мікроскопу (CryoSTM). TIA, з'єднаний з чутливим елементом (tip-sample component) CryoSTM, називається CryoSTM-TIA. Посилення його трансімпедансу є вище 1 ГОм, а пропускна здатність понад 300 кГц, але еквівалентна спектральна густина потужності вхідного шумового струму менша ніж 4 $(fA)^2$/Гц при 100 кГц. Низький шум, притаманний CryoSTM-TIA, пояснюється його конструкцією: (1) його попередній підсилювач виготовлений з пари низькошумових транзисторів з високою рухливістю електронів (HEMT); (2) шум, що генерується одним HEMT, усувається великим конденсатором; (3) ємність кабелю, що з'єднує затвор іншого HEMT з наконечником, мінімізована; (4) джерела теплового шуму, такі як резистор зворотного зв'язку, розміщуються в кріогенній зоні. Дрейф постійної вихідної напруги CryoSTM-TIA є дуже низьким, 5 мкВ/°C. Апарат може бути використаний для вимірювання сканованих тунельних спектрів диференціальної провідності, особливо сканованих тунельних спектрів дробового шуму (STSNS) квантових систем, навіть якщо дробовий шум дуже низький. Він забезпечує універсальний інструмент для вивчення різних нових квантових станів шляхом вимірювання STSNS, таких як виявлення майоранівських зв'язаних станів.

Ключові слова: кріогенний скануючий тунельний мікроскоп, підсилювач трансімпедансу, транзистори з високою рухливістю електронів, еквівалентна спектральна густина потужності вхідного шумового струму, тунельні спектри сканування дробового шуму, майоранівські зв'язані стани.